

THE LOWEST ORDER DIFFERENTIABLE FINITE ELEMENT ON RECTANGULAR GRIDS*

JUN HU[†], YUNQING HUANG[‡], AND SHANGYOU ZHANG[§]

Abstract. A macro type of biquadratic C^1 finite elements is constructed on rectangle grids. This is a rectangular version of the C^1 Powell–Sabin element, a C^1 - P_2 element on triangular grids. Here, each rectangle of the base grid is refined into four subrectangles. As in the case of the Powell–Sabin element, we have more constraints than the number of degrees of freedom on each macroelement. However, the extra constraints are consistent. It is shown further that the constructed finite element space is the full C^1 - Q_2 space on the grid. It is also shown that the finite element space is a tensor product space of one-dimensional C^1 - P_2 spaces, where the nodal basis is supported on four intervals. The B-spline function of P_2 is supported on three intervals. The Girault–Scott operator is extended to the element. The application and the convergence of the finite element to the biharmonic equation are presented. Numerical tests are provided.

Key words. differentiable finite element, biharmonic equation, Powell–Sabin element, Bogner–Fox–Schmit element, Girault–Scott operator, rectangular grids

AMS subject classifications. 65M60, 65N30

DOI. 10.1137/100806497

1. Introduction. The construction of differentiable (C^1) finite elements is relatively difficult. Most C^1 elements currently in use were constructed in 1960s and 1970s. On general triangular grids, the lowest order polynomial degree is 5 for constructing C^1 piecewise polynomials. This is the well-known Argyris P_5 element, designed in 1968 [2]. To lower the polynomial degree, the Hsieh–Clough–Tocher (HCT) P_3 macroelement was created in 1965; cf. [3]. Here each base triangle is refined into three subtriangles to form one macroelement; cf. Figure 1. Refining each base triangle into six—for example, connecting the center of the inscribed circle of a triangle to its three vertices and the centers of three neighboring triangles (cf. Figure 1)—is how the Powell–Sabin C^1 - P_2 element was created in 1977; cf. [6]. This is a revolutionary

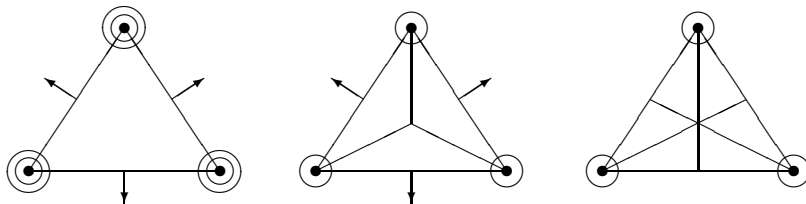


FIG. 1. C^1 - P_5 Argyris, C^1 - P_3 HCT, and C^1 - P_2 Powell–Sabin elements.

*Received by the editors August 25, 2010; accepted for publication (in revised form) April 6, 2011; published electronically July 5, 2011.

<http://www.siam.org/journals/sinum/49-4/80649.html>

[†]LMAM and School of Mathematical Sciences, Peking University, Beijing, 100871, China (hujun@math.pku.edu.cn). This author’s work was supported by NSFC project 10971005 and by A Foundation for the Author of National Excellent Doctoral Dissertation of P.R. China 200718.

[‡]Hunan Key Laboratory for Computation and Simulation in Science and Engineering, Xiangtan University, Xiangtan, Hunan, 411105, China (huangyq@xtu.edu.cn). This author’s work was supported in part by NSFC Key Project 11031006 and Hunan Provincial NSF Project 10JJ7001.

[§]Department of Mathematical Sciences, University of Delaware, Newark, DE 19716 (szhang@udel.edu).

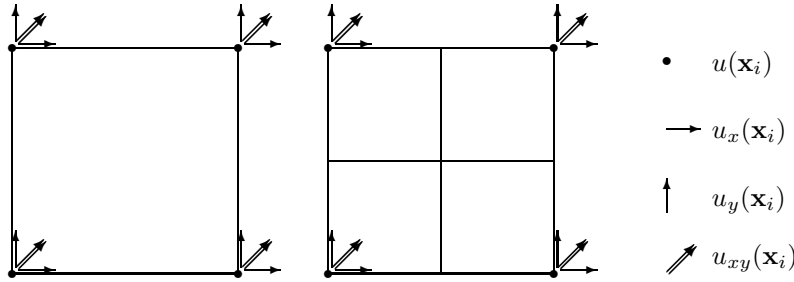


FIG. 2. The BFS Q_3 element (left) and the new C^1 - Q_2 macroelement (right).

construction in that the degree of freedom is $6 \times 6 = 36$, 6 less than that of total number of constraints, $3 \times 6 + 5 \times 3 + 3 \times 3 = 42$, on each macroelement. The extra constraints are consistent.

On rectangular grids, the Bogner–Fox–Schmit (BFS) Q_3 element was found in 1965; cf. [3]. The degree of freedom on each element for Q_3 is $4 \times 4 = 16$. The finite element function is defined by the value $u(\mathbf{x}_i)$, first derivatives $u_x(\mathbf{x}_i)$ and $u_y(\mathbf{x}_i)$, and a mixed second derivative $u_{xy}(\mathbf{x}_i)$, at four vertices, as shown in Figure 2. To lower the polynomial degree, we follow the idea of the Powell–Sabin construction. Each base rectangle is divided into four rectangles as a macroelement, as shown in Figure 2. The new C^1 - Q_2 element is depicted in Figure 2(right). We note that, similar to the Powell–Sabin P_2 element, the degrees of freedom on each macroelement are $4 \times 9 = 36$, 8 fewer than the total number of constraints $4 \times 4 + 4 \times 4 + 3 \times 4 = 44$. We show that this space is a tensor product of the one-dimensional (1D) C^1 - P_2 finite element spaces. Here we construct the (full) 1D C^1 - P_2 finite element spaces on irregular grids, where each nodal basis is supported on four intervals. The B-spline function of P_2 is supported on three intervals. That is, the traditional B-splines are adapted to form finite element spaces.

The optimal order approximation property is established for the new element. Here, the Girault–Scott operator [4] is extended/constructed for the new element so that the Girault–Scott interpolation maps H_0^2 functions to the C^1 - Q_2 finite element space. We observe from the numerical examples that the convergence rate for the error of the finite element solution is of order 3 in the L^2 norm; we cannot give a theoretical justification for it. This is a well-known problem in the finite element theory for biharmonic solutions. In addition to a useful, simpler method, the new element has its theoretic interest. Due to the nestedness of spaces in refinement, the new element has its advantages in the multigrid method and in the h -adaptive method. Another side interest is that the C^1 - Q_2 element ensures the optimal order approximation of a $Q_{2,1} \times Q_{1,2}$ divergence-free element; cf. [5, 9].

The rest of the paper has the following sections. In section 2, the full C^1 - Q_2 space and a tensor-product C^1 - Q_2 space are defined. In section 3, the equivalence of the two C^1 - Q_2 spaces is shown. In section 4, the Girault–Scott operator is introduced to show the optimal order approximation of the new finite element. The optimal order convergence for the element is proved consequently, for solving the biharmonic equation. In section 5, the 2D C^1 - Q_2 element is extended to three dimensions. In section 6, some numerical results are provided to confirm the theory.

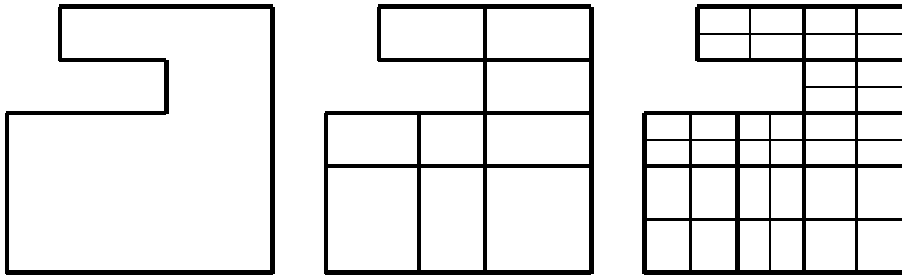


FIG. 3. A polygonal domain Ω (left), and macroelement grids \mathcal{M}_h (center) and \mathcal{T}_h (right).

2. The macro C^1 - Q_2 element. The new C^1 finite element is to be applied to the following biharmonic problem:

$$(2.1) \quad \Delta^2 u = f \quad \text{in } \Omega,$$

$$(2.2) \quad u = \partial_{\mathbf{n}} u = 0 \quad \text{on } \partial\Omega.$$

Here $\partial_{\mathbf{n}} u = \frac{\partial u}{\partial \mathbf{n}}$, Ω is a polygonal domain which can be subdivided into rectangles (cf. Figure 3), and \mathbf{n} is the unit normal vector on the boundary $\partial\Omega$. The weak form for (2.1) is: Find $u \in H_0^2(\Omega)$ such that

$$(2.3) \quad a(u, v) = (f, v) \quad \forall v \in H_0^2(\Omega).$$

Here $H_0^2(\Omega)$ is the subspace of the Sobolev space $H^2(\Omega)$ (cf. [3]) with zero boundary trace, $H_0^2(\Omega) = \{v \in H^2 \mid v = \partial_{\mathbf{n}} v = 0 \text{ on } \partial\Omega\}$, and the bilinear forms are

$$a(u, v) = \int_{\Omega} \Delta u \Delta v \, dx, \quad (f, v) = \int_{\Omega} f v \, dx.$$

Let Ω be covered exactly by a shape-regular grid \mathcal{M}_h consisting of rectangles; cf. Figure 3. We further subdivide each rectangle in grid \mathcal{M}_h into four subrectangles by a horizontal line and a vertical line. This results in a new grid \mathcal{T}_h , shown in the right diagram of Figure 3. Here the grid size h denotes the maximum dimension of all rectangles. In particular, we define eight grid sizes, $\{h_{x,i}^A, h_{y,j}^A, i, j = -2, -1, 1, 2\}$, for each internal node $A \in \mathcal{N}_h$, where \mathcal{N}_h is the set of internal grid points of the macroelement grid \mathcal{M}_h . The grid sizes are shown in Figure 4. Of course, we assume that the grids are quasi-uniform; i.e., there is a positive constant C such that

$$Ch \leq h_{x,i}^A, h_{y,j}^A \leq h.$$

Let the polynomial space of separate degree 2 or less be

$$Q_2(K) = \left\{ \sum_{0 \leq i, j \leq 2} c_{ij} x^i y^j \right\}.$$

The macro C^1 - Q_2 finite element space is defined by

$$(2.4) \quad V_h = \{v_h \in C^1(\Omega) \mid v_h|_K \in Q_2(K) \forall K \in \mathcal{T}_h, \text{ and } v_h|_{\partial\Omega} = \partial_{\mathbf{n}} v_h|_{\partial\Omega} = 0\}.$$

		$h_{y,2}^A$	
		$h_{y,1}^A$	
$h_{x,-2}^A$	$h_{x,-1}^A$	$h_{x,1}^A$	$h_{x,2}^A$
	A	$h_{y,-1}^A$	
		$h_{y,-2}^A$	

FIG. 4. The eight grid sizes associated with an internal point $A \in \mathcal{N}_h$.

The structure, nodal basis, and optimal order approximation property for this new C^1 - Q_2 element will be established later. The resulting linear system of finite element equations for (2.3) is: Find $u_h \in V_h$ such that

$$(2.5) \quad a(u_h, v_h) = (f, v_h) \quad \forall v_h \in V_h.$$

The full C^1 - Q_2 space V_h is defined abstractly in (2.4). We would find a basis for the finite element space, which can also be a tensor-product of the 1D C^1 - P_2 basis.

THEOREM 2.1. *The 1D C^1 - P_2 space on a grid $x_0 < x_1 < \dots < x_{2N+2}$,*

$$S_h = \{v \in H_0^2(x_0, x_{2N}) \mid v|_{[x_i, x_{i+1}]} \in P_2\},$$

is

$$\tilde{S}_h = \left\{ v = \sum_{i=1}^N v(x_{2i})\psi_{1,2i}(x) + v'(x_{2i})\psi_{2,2i}(x) \right\}.$$

Here the nodal basis functions are supported on four intervals (cf. Figure 5):

$$(2.6) \quad \psi_{1,2i}(x) = \begin{cases} \phi_{2,x_{2i-1}-x_{2i-2},x_{2i}-x_{2i-1}}(x-x_{2i-1}), & x_{2i-2} \leq x < x_{2i}, \\ \phi_{1,x_{2i+1}-x_{2i},x_{2i+2}-x_{2i+1}}(x-x_{2i+1}), & x_{2i} \leq x \leq x_{2i+2}, \end{cases}$$

$$(2.7) \quad \psi_{2,2i}(x) = \begin{cases} \phi_{3,x_{2i-1}-x_{2i-2},x_{2i}-x_{2i-1}}(x-x_{2i-1}), & x_{2i-2} \leq x < x_{2i}, \\ \phi_{0,x_{2i+1}-x_{2i},x_{2i+2}-x_{2i+1}}(x-x_{2i+1}), & x_{2i} \leq x \leq x_{2i+2}, \end{cases}$$

where the elementwise basis functions are defined by

$$(2.8) \quad \begin{aligned} \phi_{0,a,b}(x) &= \begin{cases} (x+a) - \frac{1}{a+b}(1 + \frac{b}{2a})(x+a)^2, & -a \leq x < 0, \\ \frac{1}{a+b} \frac{a}{2b}(b-x)^2, & 0 \leq x \leq b, \end{cases} \\ \phi_{1,a,b}(x) &= \begin{cases} 1 - \frac{1}{a+b} \frac{1}{a}(x+a)^2, & -a \leq x < 0, \\ \frac{1}{a+b} \frac{1}{b}(b-x)^2, & 0 \leq x \leq b, \end{cases} \\ \phi_{2,a,b}(x) &= \begin{cases} \frac{1}{a+b} \frac{1}{a}(x+a)^2, & -a \leq x < 0, \\ 1 - \frac{1}{a+b} \frac{1}{b}(b-x)^2, & 0 \leq x \leq b, \end{cases} \\ \phi_{3,a,b}(x) &= \begin{cases} -\frac{1}{a+b} \frac{b}{2a}(x+a)^2, & -a \leq x < 0, \\ (x-b) + \frac{1}{a+b}(1 + \frac{a}{2b})(b-x)^2, & 0 \leq x \leq b. \end{cases} \end{aligned}$$

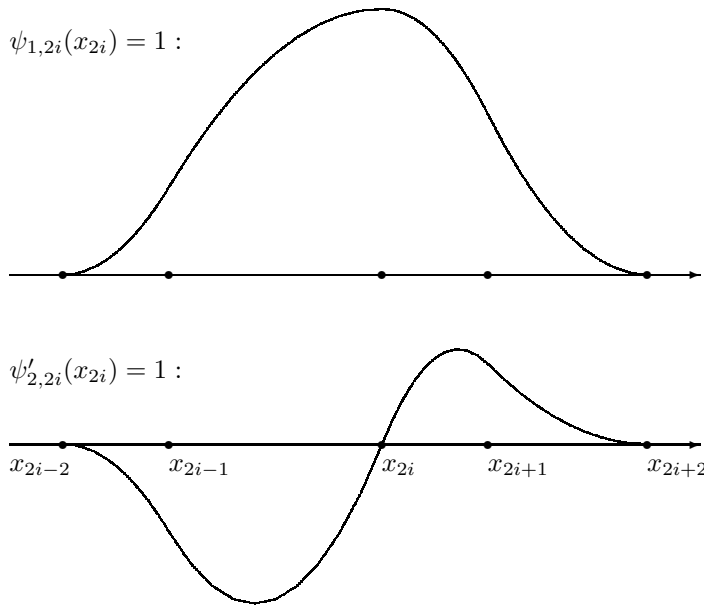


FIG. 5. Two nodal basis functions on irregular grids; cf. (2.6) and (2.7).

Proof. As a function v_h in \tilde{S}_h is C^1 and piecewise P_2 , v_h is in the space S_h by definition. That is, $\tilde{S}_h \subset S_h$. In the other direction, given a function $v_h \in S_h$, we have a unique representation

$$v_h(x) = v_h(x_{2i-2})\psi_{1,2i-2}(x) + v'_h(x_{2i-2})\psi_{2,2i-2}(x) + v_h(x_{2i})\psi_{1,2i}(x) + v'_h(x_{2i})\psi_{2,2i}(x)$$

on the interval $[x_{2i-2}, x_{2i}]$. Thus $v_h \in \tilde{S}_h$ and $S_h \subset \tilde{S}_h$. \square

For equally spaced grids in one dimension, the elementwise basis (2.8) can be defined on a reference macroelement, $[-1, 0] \cup [0, 1]$: The 1D nodal basis functions for C^1 - P_2 on the interval $[-1, 1]$ are, as depicted in Figure 6,

$$\begin{aligned}
 \phi_0(x) &= \frac{(x-1)^2}{4} - \begin{cases} x^2, & x \in [-1, 0], \\ 0, & x \in [0, 1], \end{cases} \\
 \phi_1(x) &= \frac{(x-1)^2}{2} - \begin{cases} x^2, & x \in [-1, 0], \\ 0, & x \in [0, 1], \end{cases} \\
 \phi_2(x) &= \frac{(x+1)^2}{2} - \begin{cases} 0, & x \in [-1, 0], \\ x^2, & x \in [0, 1], \end{cases} \\
 \phi_3(x) &= -\frac{(x+1)^2}{4} + \begin{cases} 0, & x \in [-1, 0], \\ x^2, & x \in [0, 1]. \end{cases}
 \end{aligned}
 \tag{2.9}$$

That is, these functions are piecewise quadratic polynomials on two intervals $[-1, 0] \cup [0, 1]$ and satisfy the conditions

$$\phi'_0(-1) = 1, \quad \phi_1(-1) = 1, \quad \phi_2(1) = 1, \quad \phi'_3(1) = 1;$$

their other nodal values are zero; and they are C^1 at $x = 0$. The same basis functions in (2.9) are constructed as before in [1]. (We found this work after we made an independent construction.) We note that the C^1 - P_2 B-spline functions were constructed a

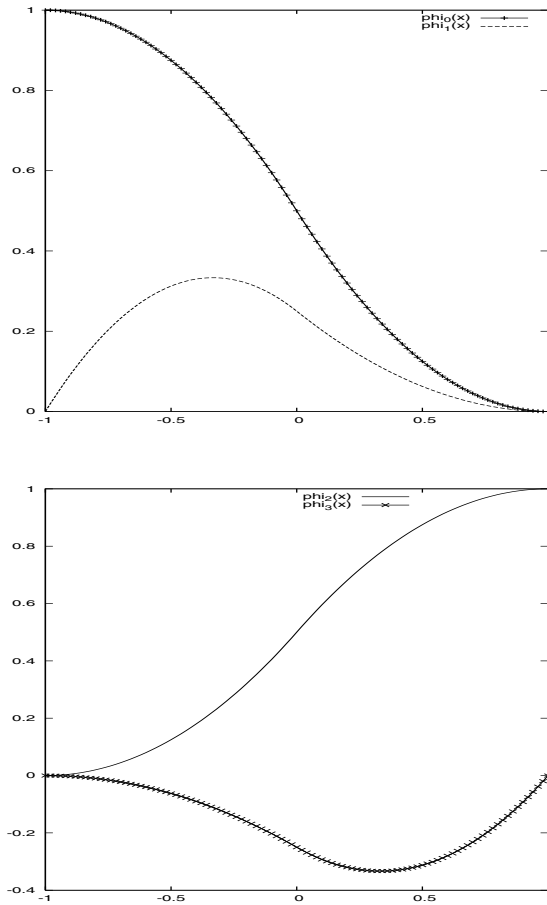


FIG. 6. The basis functions $\{\phi_i\}$ for the C^1 - P_2 space on $[-1, 0] \cup [0, 1]$; cf. (2.9).

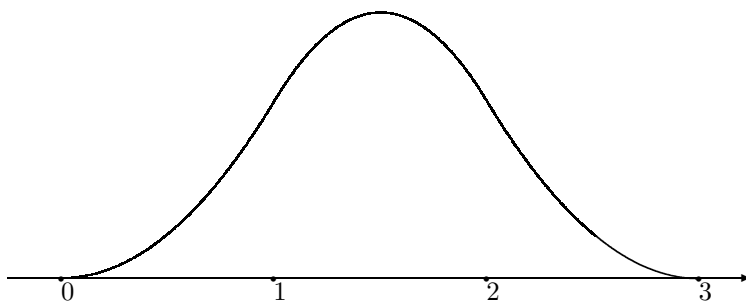


FIG. 7. A B-spline basis function; cf. (2.10).

long time ago; cf. [7]. The basis function of B-splines is supported on three intervals, as shown in Figure 7. For example, on interval $[0, 1] \cup [1, 2] \cup [2, 3]$, the B-spline basis is

$$(2.10) \quad B_2(x) = \begin{cases} 0, & x \leq 0, \\ x^2/6, & 0 < x \leq 1, \\ -x^2/3 + x - 1/2, & 1 < x \leq 2, \\ x^2/6 - x + 3/2, & 2 < x \leq 3, \\ 0, & 3 < x. \end{cases}$$

Here our nodal basis functions are constructed on four intervals, for a better fit of finite element computation. We use both the function values and the derivatives in the finite element interpolation. The typical B-spline interpolation is done by function values only, sequentially.

We next construct a 2D corresponding-tensor product basis using 1D basis functions (2.8). The 2D basis functions at a node $A = (x^A, y^A)$, of grid sizes $\{h_{x,i}^A, h_{y,j}^A\}$ (cf. Figure 4), are defined as tensor products of 1D basis functions in (2.8). We introduce some brief notation. For $i = 0, 1, 2, 3$,

$$\begin{aligned} \phi_{i,x-}^A(x) &= \phi_{i,h_{x,-2}^A, h_{x,-1}^A}(x - x^A + h_{x,-1}^A), & x \in I_{x-}^A &= [x^A - h_{x,-2}^A - h_{x,-1}^A, x^A], \\ \phi_{i,x+}^A(x) &= \phi_{i,h_{x,1}^A, h_{x,2}^A}(x - x^A - h_{x,1}^A), & x \in I_{x+}^A &= [x^A, x^A + h_{x,1}^A + h_{x,2}^A], \\ \phi_{i,y-}^A(y) &= \phi_{i,h_{y,-2}^A, h_{y,-1}^A}(y - y^A + h_{y,-1}^A), & y \in I_{y-}^A &= [y^A - h_{y,-2}^A - h_{y,-1}^A, y^A], \\ \phi_{i,y+}^A(y) &= \phi_{i,h_{y,1}^A, h_{y,2}^A}(y - y^A - h_{y,1}^A), & y \in I_{y+}^A &= [y^A, y^A + h_{y,1}^A + h_{y,2}^A]. \end{aligned}$$

Then, on 16 subrectangles, we define 4 nodal basis functions at node A :

$$(2.11) \quad \psi_1^A(x, y) = \begin{cases} \phi_{2,x-}^A(x)\phi_{2,y-}^A(y) & \text{if } (x, y) \in I_{x-}^A \times I_{y-}^A, \\ \phi_{1,x+}^A(x)\phi_{2,y-}^A(y) & \text{if } (x, y) \in I_{x+}^A \times I_{y-}^A, \\ \phi_{1,x+}^A(x)\phi_{1,y+}^A(y) & \text{if } (x, y) \in I_{x+}^A \times I_{y+}^A, \\ \phi_{2,x-}^A(x)\phi_{1,y+}^A(y) & \text{if } (x, y) \in I_{x-}^A \times I_{y+}^A, \end{cases}$$

$$(2.12) \quad \psi_2^A(x, y) = \begin{cases} \phi_{3,x-}^A(x)\phi_{2,y-}^A(y) & \text{if } (x, y) \in I_{x-}^A \times I_{y-}^A, \\ \phi_{0,x+}^A(x)\phi_{2,y-}^A(y) & \text{if } (x, y) \in I_{x+}^A \times I_{y-}^A, \\ \phi_{0,x+}^A(x)\phi_{1,y+}^A(y) & \text{if } (x, y) \in I_{x+}^A \times I_{y+}^A, \\ \phi_{3,x-}^A(x)\phi_{1,y+}^A(y) & \text{if } (x, y) \in I_{x-}^A \times I_{y+}^A, \end{cases}$$

$$(2.13) \quad \psi_3^A(x, y) = \begin{cases} \phi_{2,x-}^A(x)\phi_{3,y-}^A(y) & \text{if } (x, y) \in I_{x-}^A \times I_{y-}^A, \\ \phi_{1,x+}^A(x)\phi_{3,y-}^A(y) & \text{if } (x, y) \in I_{x+}^A \times I_{y-}^A, \\ \phi_{1,x+}^A(x)\phi_{0,y+}^A(y) & \text{if } (x, y) \in I_{x+}^A \times I_{y+}^A, \\ \phi_{2,x-}^A(x)\phi_{0,y+}^A(y) & \text{if } (x, y) \in I_{x-}^A \times I_{y+}^A, \end{cases}$$

$$(2.14) \quad \psi_4^A(x, y) = \begin{cases} \phi_{3,x-}^A(x)\phi_{3,y-}^A(y) & \text{if } (x, y) \in I_{x-}^A \times I_{y-}^A, \\ \phi_{0,x+}^A(x)\phi_{3,y-}^A(y) & \text{if } (x, y) \in I_{x+}^A \times I_{y-}^A, \\ \phi_{0,x+}^A(x)\phi_{0,y+}^A(y) & \text{if } (x, y) \in I_{x+}^A \times I_{y+}^A, \\ \phi_{3,x-}^A(x)\phi_{0,y+}^A(y) & \text{if } (x, y) \in I_{x-}^A \times I_{y+}^A. \end{cases}$$

These basis functions satisfy

$$\psi_1^A(x^A, y^A) = 1, \quad \partial_x \psi_2^A(x^A, y^A) = 1, \quad \partial_y \psi_3^A(x^A, y^A) = 1, \quad \partial_{xy} \psi_4^A(x^A, y^A) = 1.$$

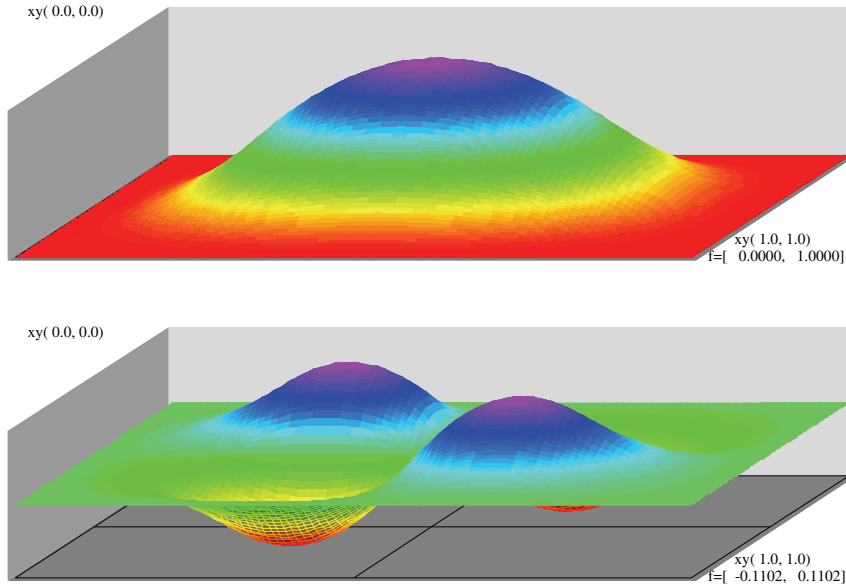


FIG. 8. Two nodal basis functions, ψ_1^A (top) and ψ_4^A (bottom) defined in (2.11) and (2.14), respectively.

The nodal values are zero at rest nodes of \mathcal{N}_h . In particular, ψ_1 and ψ_4 are shown in Figure 8, on a uniform grid.

Via the basis functions (2.11)–(2.14), we define another finite element space, which will be shown to be the same as the full C^1 - Q_2 space V_h , defined in (2.4):

$$(2.15) \quad \tilde{V}_h = \left\{ v_h(x, y) = \sum_{A \in \mathcal{N}_h} \sum_{i=1}^4 v_i^A \psi_i^A(x, y), (x, y) \in \Omega \right\}.$$

Here in (2.15), the coefficients are the nodal values of the C^1 function v_h ,

$$v_i^A = \begin{cases} v_h(x^A, y^A), & i = 1, \\ \partial_x v_h(x^A, y^A), & i = 2, \\ \partial_y v_h(x^A, y^A), & i = 3, \\ \partial_{xy}^2 v_h(x^A, y^A), & i = 4. \end{cases}$$

This relationship also defines an interpolation operator $I_h : C_0^1(\Omega) \cap C^2(\Omega) \rightarrow \tilde{V}_h$ by

$$(2.16) \quad I_h v = \sum_{A \in \mathcal{N}_h} v(x^A, y^A) \psi_1^A(x, y) + v_x(x^A, y^A) \psi_2^A(x, y) + v_y(x^A, y^A) \psi_3^A(x, y) + v_{xy}(x^A, y^A) \psi_4^A(x, y).$$

In other words, the finite element function is determined by its four nodal values at the internal grid points of the macroelement grid \mathcal{M}_h , shown in Figure 9.

LEMMA 2.1. The finite element space \tilde{V}_h , defined in (2.15), is of C^1 and

$$\tilde{V}_h \subset V_h.$$

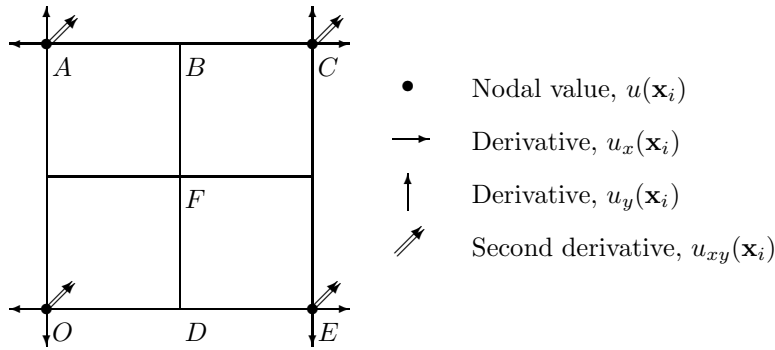


FIG. 9. Degrees of freedom for the macro C^1 - Q_2 element.

Proof. All the basis functions $\psi_i^A(x, y)$ are tensor products of 1D C^1 functions on each of four 4-square patches, $I_{x\pm}^A \times I_{y\pm}^A$. In addition, such basis functions are C_0^1 on the boundary, i.e.,

$$(2.17) \quad \psi_i^A(x, y) \in C_0^1\left(\left(I_{x-}^A \cup I_{x+}^A\right) \times \left(I_{y-}^A \cup I_{y+}^A\right)\right).$$

To show (2.17), by symmetry, we need only to show that $\psi_i^A(x, y)$ is C^1 at edge AC and BD , and C_0^1 at edge CE ; cf. Figure 9. That is, we are required to show only that

$$\begin{aligned} \psi_i^A(x, y_+^A) &= \psi_i^A(x, y_-^A) & \forall x \in I_{x+}^A, \\ \partial_y \psi_i^A(x, y_+^A) &= \partial_y \psi_i^A(x, y_-^A) & \forall x \in I_{x+}^A, \\ \psi_i^A(x_+^A + h_{x,1}^A, y) &= \psi_i^A(x_-^A + h_{x,1}^A, y) & \forall y \in I_{y-}^A, \\ \partial_x \psi_i^A(x_+^A + h_{x,1}^A, y) &= \partial_x \psi_i^A(x_-^A + h_{x,1}^A, y) & \forall y \in I_{y-}^A, \\ \psi_i^A(x_-^A + h_{x,1}^A + h_{x,2}^A, y) &= 0 & \forall y \in I_{y-}^A, \\ \partial_x \psi_i^A(x_-^A + h_{x,1}^A + h_{x,2}^A, y) &= 0 & \forall y \in I_{y-}^A. \end{aligned}$$

Here x_{\pm}^A denote the limits from two sides, $x_{\pm}^A = \lim_{x \rightarrow \pm 0} (x^A + x)$. We verify only the first equation and the third equation with $i = 1$. All the rest are shown exactly the same way. By (2.11) (cf. Figures 4 and 9), for $x \in I_{x+}^A$,

$$\begin{aligned} \psi_1^A(x, y_+^A) &= \phi_{1,x+}^A(x) \phi_{1,y+}^A(y^A) = \phi_{1,x+}^A(x) \phi_{1,h_{y,1}^A, h_{y,2}^A}(-h_{y,1}^A) \\ &= \phi_{1,x+}^A(x), \\ \psi_1^A(x, y_-^A) &= \phi_{1,x+}^A(x) \phi_{2,y-}^A(y^A) = \phi_{1,x+}^A(x) \phi_{2,h_{y,-2}^A, h_{y,-1}^A}(h_{y,2}^A) \\ &= \phi_{1,x+}^A(x) = \psi_1^A(x, y_+^A). \end{aligned}$$

For the third equation, inside a macroelement $I_{x+}^A \times I_{y-}^A$ of \mathcal{M}_h , it is trivial because of the way that the 1D C^1 basis functions are defined; see (2.8). For $y \in I_{y-}^A$,

$$\begin{aligned} \psi_1^A(x_+^A + h_{x,1}^A, y) &= \phi_{1,x+}^A(x^A + h_{x,1}^A) \phi_{2,y-}^A(y) \\ &= \phi_{1,h_{x,1}^A, h_{x,2}^A}(0) \phi_{2,y-}^A(y) = \frac{h_{x,2}^A}{h_{x,1}^A + h_{x,2}^A} \phi_{2,y-}^A(y), \\ \psi_1^A(x_-^A + h_{x,1}^A, y) &= \phi_{1,x+}^A(x^A + h_{x,1}^A) \phi_{2,y-}^A(y) = \psi_1^A(x_+^A + h_{x,1}^A, y). \end{aligned}$$

As $\psi_i^A(x, y)$ is zero outside its support, by (2.17), $\psi_i^A(x, y) \in C_0^1(\Omega)$. As all basis functions are $C_0^1(\Omega)$, any linear combination

$$\left(\sum_{A \in \mathcal{N}_h} \sum_{i=1}^4 v_i^A \psi_i^A(x, y) \right) = v_h \in C_0^1(\Omega).$$

That is, $\tilde{V}_h \subset C_0^1(\Omega)$. As V_h is defined as the whole C^1 - Q_2 space on \mathcal{T}_h , it follows that it contains the C^1 - Q_2 space \tilde{V}_h as its subspace, i.e., $\tilde{V}_h \subset V_h$. \square

3. The full C^1 - Q_2 space. The most C^1 finite element spaces in use are only subspaces of the corresponding C^1 piecewise polynomial spaces. For example, the Argyris finite element space is a subspace of the C^1 - P_5 space on a triangular grid, where the nodal continuity is of C^2 . It is important in its applications to other polynomial approximation problems that the finite element space constructed be a full C^1 space. One important application is to the divergence-free C^0 finite element on rectangular grids [5].

So far, we have defined two C^1 - Q_2 finite element spaces, V_h and \tilde{V}_h . V_h is defined abstractly. Roughly speaking, a Q_2 polynomial has $3 \times 3 = 9$ degrees of freedom, but it is required to satisfy at least $4 \times 4 = 16$ constraints to fulfill the nodal C^1 continuity requirement. Even if we decide to form V_h on 2×2 macroelement grids, there would be still more constraints than degrees of freedom on each 2×2 patch. We have $4 \times 9 = 36$ degrees of freedom on each patch for piecewise Q_2 polynomials. But we have a total of 4×4 (C^1 requirements at 4 corners) + 3×4 (C^1 requirements at the center vertex) + 4×4 (C^1 requirements at the 4 midedge vertices) = 44 constraints. We avoid this difficulty partially by constructing another C^1 - Q_2 subspace \tilde{V}_h , via tensor-product. After showing $\tilde{V}_h \subset V_h$ in Lemma 2.1, we would face the above difficulty in showing $\tilde{V}_h \supset V_h$, i.e., showing that those 36 degrees of freedom do uniquely satisfy the 44 constraints. In other words, a C^1 - Q_2 function is uniquely defined by the 16 degrees of freedom (shown in Figure 9) on each macroelement in \mathcal{M}_h . This is how we discovered the new C^1 - Q_2 element. But we prove this indirectly via the tensor-product of 1D C^1 - P_2 functions.

THEOREM 3.1. *The full C^1 - Q_2 space V_h of (2.4) is characterized by the tensor-product space \tilde{V}_h (2.15):*

$$V_h = \tilde{V}_h.$$

Proof. By Lemma 2.1, we are left to show $V_h \subset \tilde{V}_h$. Let $v_h \in V_h$. We show $v_h \in \tilde{V}_h$ by showing $I_h v_h = v_h$, where I_h is a nodal-value interpolation operator defined in (2.16). First, we show that I_h is well defined on V_h . Please note that I_h is defined for C^2 functions in (2.16). We need to show that the four values $\partial_{xy} v_h(x_{\pm}^E, y_{\pm}^E)$ are the same at all vertexes of \mathcal{T}_h , such as L and E in Figure 10. We take the vertex L as an example to show this fact. Because $\partial_y v_h$ is continuous on edge KL , by Lemma 2.1, $\partial_{xy} v_h$ is the same on both sides of edge KL . In particular,

$$\partial_{xy} v_h|_{BJLK}(L) = \partial_{xy} v_h|_{KLNE}(L).$$

We show next that $w_h := I_h v_h - v_h \equiv 0$ on one macroelement $BCFE$; cf. Figure 10. For simplicity of notation, we map $BCFE$ to the reference element $[-1, 1]^2$ using four scaling maps. Restricting w_h to edge BC , it is a two-piece P_2 polynomial.

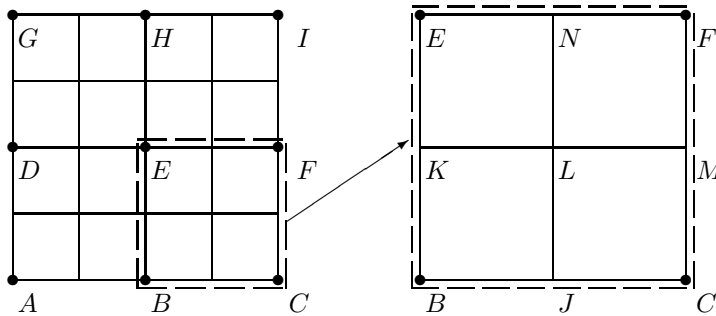


FIG. 10. Vertices on four macroelements (left) and on one macroelement (right).

Because $w_h(\pm 1) = \partial_x w_h(\pm 1) = 0$, it follows that

$$w_h|_{BC} = \begin{cases} c_1(x + 1)^2, & x \in [-1, 0], \\ c_2(x - 1)^2, & x \in [0, 1], \end{cases}$$

for some constants c_1 and c_2 . By the continuity of $w_h|_{BC}$ at midpoint J (cf. Figure 10), $c_1 = c_2$. Then, by the continuity of $\partial_x w_h|_{BC}$ at midpoint J , $c_1 = 0$. Thus $w_h|_{BC} \equiv 0$. Next, similarly, we get $\partial_y w_h|_{BC} \equiv 0$, as it is also a two-piece P_2 polynomial. Thus, we can factor out the two factors to have

$$w_h|_{BJLK} = (y + 1)^2 p_2(x)$$

for some quadratic polynomial $p_2(x)$. Symmetrically, $w_h = \partial_x w_h = 0$ when restricted to the vertical edge BK . Repeating this process at the other three vertices C, F , and E , it follows that

$$w_h|_{BCFE} = \begin{cases} C_1(x + 1)^2(y + 1)^2, & (x, y) \in [-1, 0] \times [-1, 0], \\ C_2(x - 1)^2(y + 1)^2, & (x, y) \in [0, 1] \times [-1, 0], \\ C_3(x - 1)^2(y - 1)^2, & (x, y) \in [0, 1] \times [0, 1], \\ C_4(x + 1)^2(y - 1)^2, & (x, y) \in [-1, 0] \times [0, 1], \end{cases}$$

for some constants C_i . By the continuity of w_h at the center point L , $C_1 = C_2 = C_3 = C_4$. Then, by the continuity of ∇w_h at L , $C_1 = 0$. Hence $w_h \equiv 0$, and thus $v_h \in \tilde{V}_h$. \square

Though $\tilde{V}_h = V_h$ is the maximum C^1 - Q_2 space, we still have to show that it contains the Q_2 polynomials locally, due to the use of a macrogrid.

PROPOSITION 3.1. For all $u \in H^{3+\epsilon}(\Omega) \cap H_0^2(\Omega)$, $I_h u \in \tilde{V}_h$. If $u|_M \in Q_2$ for some $M \in \mathcal{M}_h$, in addition, then

$$(3.1) \quad I_h u|_M = u|_M.$$

Here the interpolation operator I_h is defined in (2.16).

Proof. $I_h u$ is well defined for an $H^{3+\epsilon}$ function u , as the values of u, u_x, u_y , and u_{xy} are well defined at internal and boundary vertices, by the Sobolev embedding theorem. Then, with a boundary condition of $H_0^2(\Omega)$, we have $I_h u \in V_h$. We show next that I_h preserves Q_2 polynomials locally. This is in fact implied by Theorem 3.1,

except for a simple modification on the boundary condition. However, we give another direct proof.

On one macroelement M of four rectangles, $I_{x^+}^A \times I_{y^-}^A$, shown in Figure 9, we verify $I_h v = v$ for $v = 1$. By (2.16), (2.11)–(2.12), and (2.8),

$$\begin{aligned} I_h 1 &= \psi_1^A(x, y) + \psi_1^C(x, y) + \psi_1^E(x, y) + \psi_1^O(x, y) \\ &= \phi_{1, h_{x,1}^A, h_{x,2}^A}(x - x^F) \phi_{2, h_{y,-2}^A, h_{y,-1}^A}(y - y^F) \\ &\quad + \phi_{2, h_{x,-2}^C, h_{x,-1}^C}(x - x^F) \phi_{2, h_{y,-2}^C, h_{y,-1}^C}(y - y^F) \\ &\quad + \phi_{2, h_{x,-2}^E, h_{x,-1}^E}(x - x^F) \phi_{1, h_{y,1}^E, h_{y,2}^E}(y - y^F) \\ &\quad + \phi_{1, h_{x,1}^O, h_{x,2}^O}(x - x^F) \phi_{1, h_{y,1}^O, h_{y,2}^O}(y - y^F) \\ &= [\phi_{1, h_{x,1}^A, h_{x,2}^A}(x - x^F) + \phi_{2, h_{x,1}^A, h_{x,2}^A}(x - x^F)] \\ &\quad \cdot [\phi_{1, h_{y,-2}^A, h_{y,-1}^A}(y - y^F) + \phi_{1, h_{y,-2}^A, h_{y,-1}^A}(y - y^F)]. \end{aligned}$$

That is, an interpolation of a tensor product is the tensor product of the one-directional interpolations. Note that $h_{x,1}^A = h_{x,1}^O = h_{x,-2}^C = h_{x,-2}^E$. So we need only to verify the polynomial preserving property of I_h in the 1D interpolation. By the definition (2.8), we can see the following equalities by simple cancellation:

$$\begin{aligned} \phi_{1,a,b}(x) + \phi_{2,a,b}(x) &= 1, \\ -a\phi_{1,a,b}(x) + b\phi_{2,a,b}(x) &= \begin{cases} -a + \frac{(x+a)^2}{a}, & x < 0, \\ b - \frac{(b-x)^2}{b}, & x > 0, \end{cases} \\ a^2\phi_{1,a,b}(x) + b^2\phi_{2,a,b}(x) &= \begin{cases} a^2 + \frac{(b-a)(x+a)^2}{a}, & x < 0, \\ b^2 + \frac{(a-b)(b-x)^2}{b}, & x > 0, \end{cases} \\ \phi_{0,a,b}(x) + \phi_{3,a,b}(x) &= \begin{cases} (x+a) - \frac{(x+a)^2}{a}, & x < 0, \\ (x-b) + \frac{(b-x)^2}{b}, & x > 0, \end{cases} \\ -a\phi_{0,a,b}(x) + b\phi_{3,a,b}(x) &= \begin{cases} -a(x+a) + \frac{(2a-b)(x+a)^2}{2a}, & x < 0, \\ b(x-b) + \frac{(2b-a)(b-x)^2}{2b}, & x > 0. \end{cases} \end{aligned}$$

Thus, using the nodal values at the end points, we get, for $x \in [x^F - h_{x,1}^A, x^F + h_{x,2}^A]$,

$$\begin{aligned} I_h 1 &= \phi_{1, h_{x,1}^A, h_{x,2}^A}(x - x^F) + \phi_{2, h_{x,1}^A, h_{x,2}^A}(x - x^F) = 1, \\ I_h x &= I_h x^F + I_h(x - x^F) \\ &= x^F - h_{x,1}^A \phi_{1, h_{x,1}^A, h_{x,2}^A}(x - x^F) + \phi_{0, h_{x,1}^A, h_{x,2}^A}(x - x^F) \\ &\quad + \phi_{3, h_{x,1}^A, h_{x,2}^A}(x - x^F) + h_{x,2}^A \phi_{2, h_{x,1}^A, h_{x,2}^A}(x - x^F) \\ &= x^F + (x - x^F) = x \end{aligned}$$

and

$$\begin{aligned}
 I_h x^2 &= I_h(x^F)^2 + I_h 2x^F(x - x^F) + I_h(x - x^F)^2 \\
 &= (x^F)^2 + 2x^F(x - x^F) \\
 &\quad + (h_{x,1}^A)^2 \phi_{1,h_{x,1}^A,h_{x,2}^A}(x - x^F) - 2h_{x,1}^A \phi_{0,h_{x,1}^A,h_{x,2}^A}(x - x^F) \\
 &\quad + 2h_{x,2}^A \phi_{3,h_{x,1}^A,h_{x,2}^A}(x - x^F) + (h_{x,2}^A)^2 \phi_{2,h_{x,1}^A,h_{x,2}^A}(x - x^F) \\
 &= (x^F)^2 + 2x^F(x - x^F) \\
 &\quad + \begin{cases} (h_{x,1}^A)^2 - 2h_{x,1}^A(x - x^A) + (x - x^A)^2, & x < x^F, \\ (h_{x,2}^A)^2 + 2h_{x,2}^A(x - x^C) + (x - x^C)^2, & x > x^F, \end{cases} \\
 &= (x^F)^2 + 2x^F(x - x^F) + (x - x^F)^2 = x^2. \quad \square
 \end{aligned}$$

4. The optimal order approximation. We would apply the Girault–Scott operator [4] to show the optimal order approximation of the space V_h . A reason for extending the nodal interpolation operator I_h to the Girault–Scott operator \tilde{I}_h is the use of u_{xy} as a nodal value, which requires $H^{3+\epsilon}$ regularity for the function u . We would assume H^2 regularity for the biharmonic solution u in (2.1). The Girault–Scott operator defines an interpolation $\tilde{I}_h u$ using only the traces of u and $\partial_n u$ on some edges, which are $H^{3/2}$ and $H^{1/2}$ functions. Then the finite element solution approximates the weak solution u in the optimal order, following the C ea lemma.

The Girault–Scott [4] operator defines nodal values by averaging the function on an edge attached to the vertex. In Figure 11, we display such a selection. For a vertex A at the boundary, the edge σ_A to be selected must be a boundary edge. This is to ensure that the boundary conditions would be kept after interpolation. At an internal vertex B , any of the four edges attached to B can be chosen as σ_B .

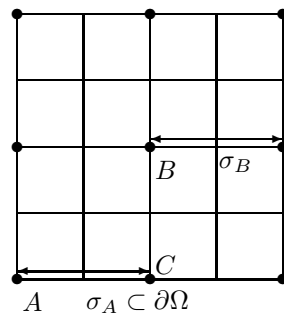


FIG. 11. The averaging edge for the Girault–Scott operator at a vertex A or B .

Let us assume that σ_A is a horizontal edge for simplicity. When restricting the basis functions $\{\psi_k^A\}$ to a horizontal edge σ_A , we have two 1D basis functions (cf. (2.11) and (2.12)):

$$\phi_{1,x^+}^A(x) \text{ and } \phi_{0,x^+}^A(x).$$

However, a V_h function v_h on σ_A also depends on its nodal values on the other end of σ_A , C , shown in Figure 11. The restrictions on σ_A for the two basis functions at the other end point of σ_A are

$$\phi_{2,x^+}^A(x) \text{ and } \phi_{3,x^+}^A(x).$$

For these four linearly independent (in $L^2([x^A, x^C])$) functions, we can define a dual basis

$$\{\psi_k^d(x) \in C^1([x^A, x^C]) \mid \psi_k^d|_{[x^A, x^A+h_{x,1}^A]} \in P_2, \psi_k^d|_{[x^A+h_{x,1}^A, x^C]} \in P_2, k = 0, 1, 2, 3\}$$

such that

$$(4.1) \quad \int_{x^A}^{x^C} \psi_0^d(x) \phi_{k,x^+}^A(x) dx = \begin{cases} 1, & k = 1, \\ 0, & k = 0, 2, 3, \end{cases}$$

$$(4.2) \quad \int_{x^A}^{x^C} \psi_1^d(x) (x - x^A)(x - x^C) \frac{d}{dx} \phi_{k,x^+}^A(x) dx = \begin{cases} 1, & k = 0, \\ 0, & k = 1, 2, 3. \end{cases}$$

Via a symbolic computation, we can get, on the reference element,

$$(4.3) \quad \psi_0^d = -\frac{3}{4} + 6x + \begin{cases} 55x^2/4, & x \in [-1, 0], \\ -25x^2/4, & x \in [0, 1], \end{cases}$$

$$(4.4) \quad \psi_1^d = \frac{9}{8} + \begin{cases} -123x^2/8, & x \in [-1, 0], \\ -27x^2/8, & x \in [0, 1]. \end{cases}$$

By appropriate scaling mappings, we can find the true dual basis defined on $[x^A, x^A + h_{x,1}^A] \cup [x^A + h_{x,1}^A, x^C]$. $\psi_0^d(x)$ has $O(1)$ scalings on the two intervals, but $\psi_0^d(x)$ has $O(h^{-1})$ scalings. The other two dual basis functions, ψ_2^d and ψ_3^d , for the other end point C , satisfy the other two orthogonal relations, similar to (4.1) and (4.2).

The Girault–Scott operator is defined as

$$(4.5) \quad \begin{aligned} \tilde{I}_h : H_0^2(\Omega) &\rightarrow V_h, \\ u &\rightarrow v = \tilde{I}_h u, \end{aligned}$$

where the nodal values of v are defined by

$$\begin{aligned} v(A) &= \int_{\sigma_A} \psi_0^d(x) u(x, y^A) dx, \\ v_x(A) &= - \int_{\sigma_A} \frac{d}{dx} \left(\psi_1^d(x) (x - x^A)(x - x^C) \right) u(x, y^A) dx, \\ v_y(A) &= \int_{\sigma_A} \psi_0^d(x) u_y(x, y^A) dx, \\ v_{xy}(A) &= - \int_{\sigma_A} \frac{d}{dx} \left(\psi_1^d(x) (x - x^A)(x - x^C) \right) u_y(x, y^A) dx. \end{aligned}$$

Please note that the averaging is done only on u and u_y , but not on u_{xy} . For the two nodal values $v_x(A)$ and $v_{xy}(A)$, we use integration by parts when doing averaging of u and u_y on σ_A . This is the beauty of the Girault–Scott operator [4].

LEMMA 4.1. \tilde{I}_h preserves V_h functions; i.e.,

$$(4.6) \quad \tilde{I}_h v_h = v_h \quad \forall v_h \in V_h.$$

Proof. Let $v_h \in V_h$ be expressed as

$$v_h(x, y) = \sum_{A \in \mathcal{N}_h} \sum_{k=1}^4 v_k^A \psi_k^A(x, y).$$

We want to show that \tilde{I}_h preserves each term of v_h in the expansion. That is, we show that \tilde{I}_h preserves the nodal values of v_h :

$$\begin{aligned}\tilde{I}_h v_h(A) &= v_h(A), & (\tilde{I}_h v_h)_x(A) &= \frac{\partial}{\partial x} v_h(A), \\ (\tilde{I}_h v_h)_y(A) &= \frac{\partial}{\partial y} v_h(A), & (\tilde{I}_h v_h)_{xy}(A) &= \frac{\partial^2}{\partial x \partial y} v_h(A).\end{aligned}$$

Since all other terms involved on the edge vanish by (4.5), (4.1)–(4.2), (2.16), and the definitions of $\phi_{k,x+}^A$, $k = 0, 1, 2, 3$, and of ψ_k^A , $k = 1, 2, 3, 4$, we get (cf. Figure 11)

$$\begin{aligned}\tilde{I}_h v_h(A) &= \int_{\sigma_A} \psi_0^d(x) v_h(x, y^A) dx \\ &= \int_{\sigma_A} \psi_0^d(x) \sum_{k=1,2} \left(v_k^A \psi_k^A(x, y^A) + v_k^C \psi_k^C(x, y^A) \right) dx \\ &= \int_{\sigma_A} \psi_0^d(x) v_1^A \phi_{1,x+}^A(x) dx \\ &= v_1^A = v_h(A).\end{aligned}$$

Next we show $(\tilde{I}_h v_h)_x(A) = (\partial v_h / \partial x)(A)$:

$$\begin{aligned}(\tilde{I}_h v_h)_x(A) &= - \int_{\sigma_A} \frac{d}{dx} \left(\psi_1^d(x) (x - x^A)(x - x^C) \right) v_h(x, y^A) dx \\ &= \int_{\sigma_A} \psi_1^d(x) (x - x^A)(x - x^C) \frac{d}{dx} v_h(x, y^A) dx \\ &= \int_{\sigma_A} \psi_1^d(x) (x - x^A)(x - x^C) \sum_{k=1,2} \frac{d}{dx} \left(v_k^A \psi_k^A(x, y^A) + v_k^C \psi_k^C(x, y^A) \right) dx \\ &= \int_{\sigma_A} \psi_1^d(x) (x - x^A)(x - x^C) v_2^A \frac{d}{dx} \phi_{0,x+}^A(x) dx \\ &= v_2^A = \frac{\partial}{\partial x} v_h(A).\end{aligned}$$

For the third term, we can get

$$\begin{aligned}(\tilde{I}_h v_h)_y(A) &= \int_{\sigma_A} \psi_0^d(x) \frac{d}{dy} v_h(x, y^A) dx \\ &= \int_{\sigma_A} \psi_0^d(x) \sum_{k=3,4} \frac{d}{dy} \left(v_k^A \psi_k^A(x, y^A) + v_k^C \psi_k^C(x, y^A) \right) dx \\ &= \int_{\sigma_A} \psi_0^d(x) v_3^A \phi_{1,x+}^A(x, y^A) dx \\ &= v_3^A = \frac{\partial}{\partial y} v_h(A).\end{aligned}$$

For the last term of the high-order derivative, we also need an integration by parts:

$$\begin{aligned}
 (\tilde{I}_h v_h)_{xy}(A) &= - \int_{\sigma_A} \frac{d}{dx} \left(\psi_1^d(x)(x-x^A)(x-x^C) \right) \frac{d}{dy} v_h(x, y^A) dx \\
 &= \int_{\sigma_A} \psi_1^d(x)(x-x^A)(x-x^C) \frac{\partial^2}{\partial x \partial y} v_h(x, y^A) dx \\
 &= \int_{\sigma_A} \psi_1^d(x)(x-x^A)(x-x^C) \\
 &\quad \cdot \sum_{k=3,4} \frac{\partial^2}{\partial x \partial y} \left(v_k^A \psi_k^A(x, y^A) + v_k^C \psi_k^C(x, y^A) \right) dx \\
 &= \int_{\sigma_A} \psi_1^d(x)(x-x^A)(x-x^C) v_4^A \frac{d}{dx} \phi_{0,x^+}^A(x) dx \\
 &= v_4^A = \frac{\partial^2}{\partial x \partial y} v_h(A).
 \end{aligned}$$

Here $\sigma_A = AC$ is an edge at A , as shown in Figure 11. □

We show the approximation property of the finite element space by the local Q_2 -preservation of the nodal interpolation operator I_h and the V_h -preservation of the Girault–Scott operator \tilde{I}_h .

THEOREM 4.1. *For all $u \in H_0^2(\Omega)$, $\tilde{I}_h u \in \tilde{V}_h$ and*

$$(4.7) \quad \|u - \tilde{I}_h u\|_{L^2} + h \|u - \tilde{I}_h u\|_{H^1} + h^2 \|u - \tilde{I}_h u\|_{H^2} \leq Ch^2 |u|_{H^2}.$$

Here the interpolation operator \tilde{I}_h is defined in (4.5).

Proof. It is standard to show the stability of operator \tilde{I}_h . For details, we refer to [4, 8]. If $u \in H_0^2(\Omega)$ is also a Q_2 function locally, $u|_M \in Q_2$ for some $M \in \mathcal{M}_h$, by (3.1) and (4.6),

$$\tilde{I}_h u \Big|_M = \tilde{I}_h(I_h u) \Big|_M = I_h u \Big|_M = u \Big|_M.$$

Thus (4.7) follows after applying the Bramble–Hilbert lemma; cf. [4, 8]. □

We finish the analysis with the convergence theorem.

THEOREM 4.2. *The discrete solution u_h of (2.5) approximates that of (2.1) in the optimal order:*

$$(4.8) \quad |u - u_h|_{H^1(\Omega)} + h^r |u - u_h|_{H^2(\Omega)} \leq Ch^{\min\{2, 2r\}} |u|_{H^{2+r}(\Omega)}, \quad 0 < r \leq 1.$$

Proof. The proof is standard, using the Céa lemma for the H^2 norm. For the H^1 norm estimate, a duality argument is applied. See [3] for details. □

5. The 3D C^1 - Q_2 finite element. In this section, we extend our 2D C^1 - Q_2 finite element to three dimensions. The extension is straightforward, by the 3D tensor-product. The domain is subdivided using a macroelement grid \mathcal{M}_h . Each cuboid of the rectangular grid \mathcal{M}_h is subdivided into eight cuboids to form the computational grid \mathcal{T}_h ; cf. Figure 12.

The finite element space is defined by

$$\begin{aligned}
 V_h &= \{v_h \in C^1(\Omega) \cap H_0^2(\Omega) \mid v_h|_K \in Q_2 \quad \forall K \in \mathcal{T}_h\} \\
 &= \left\{ v(x, y, z) = \sum_{A \in \mathcal{N}_h} \sum_{l=1}^8 v_l^A \psi_l^A(x, y, z) \right\},
 \end{aligned}$$

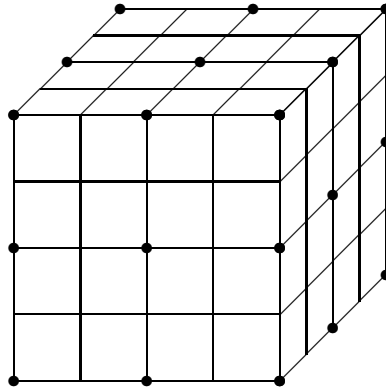


FIG. 12. A $4 \times 4 \times 4$ grid in three dimensions and its boundary C^1 - Q_2 nodes.

where \mathcal{N}_h is the set of all internal nodes of \mathcal{M}_h . The equivalence of the two definitions above can be shown using a similar argument in Theorem 3.1. Depending on which subcuboid is analyzed (cf. (2.11)–(2.14)), the eight nodal basis functions are defined by tensor products,

$$\psi_l^A(x, y, z) = \phi_{i,x\pm}^A(x)\phi_{j,y\pm}^A(y)\phi_{k,z\pm}^A(z).$$

At each node, the eight coefficients are (cf. (2.16))

$$v(A), v_x(A), v_y(A), v_z(A), v_{xy}(A), v_{yz}(A), v_{xz}(A), v_{xyz}(A).$$

The analysis in two dimensions can be extended to this 3D element straightforwardly.

6. Numerical tests. In this section, we report some simple numerical tests on the new C^1 - Q_2 element for solving the biharmonic equation (2.1). We choose the exact solution in (2.1) as

$$(6.1) \quad u(x, y) = 2^8 x^2(1-x)^2 y^2(1-y)^2.$$

The first three levels of grid \mathcal{T}_h are depicted in Figure 13; i.e., each square is refined into four subsquares in the next level. The initial or level-one grid is simply one unit square. Thus $V_h = \{0\}$ on level one. The numerical solution and the nodal error are plotted in Figure 14. It is also interesting to view the derivative errors in Figure 15, which may help us to find some recovering methods for superconvergence.

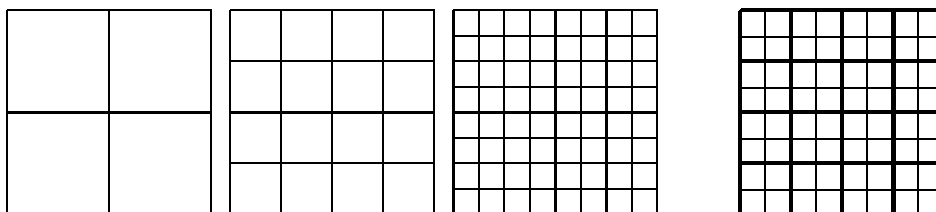


FIG. 13. Three levels of nestedly refined grids, and a macroelement grid.

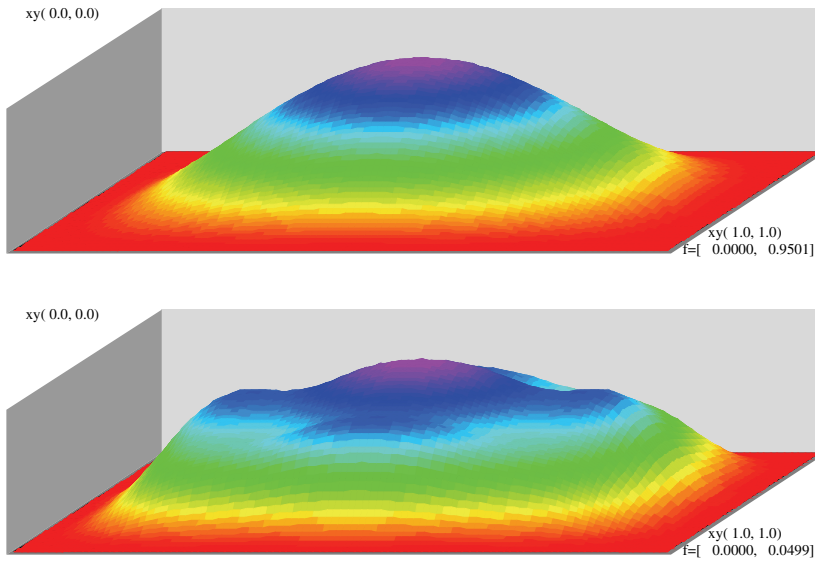


FIG. 14. The solution u_h and its error $u - u_h$ for (6.1) at level 3.

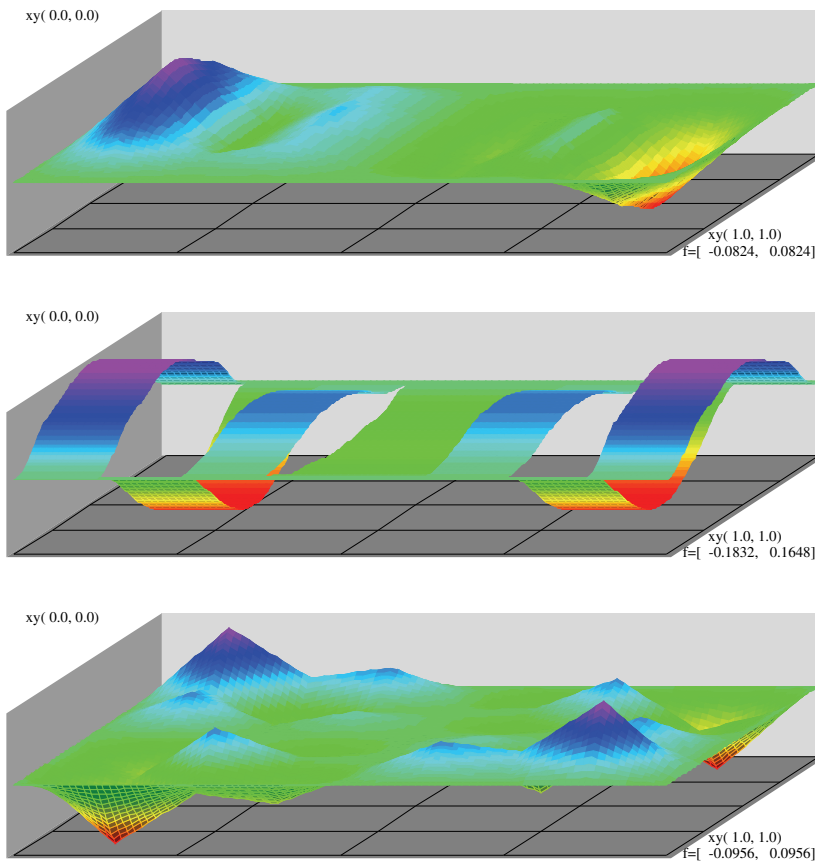


FIG. 15. $(u - u_h)_x$, $(u - u_h)_{xx}$, and $(u - u_h)_{xy}$ for (6.1) at level 3.

The discrete finite element equations are solved by conjugate gradient iteration. The number of iterations is listed in the last column of Table 1. In Table 1, we can find the orders of convergence of the finite element solutions in the H^2 and H^1 norms. They fit the analytic result, Theorem 4.2. Surprisingly, we find that the L^2 convergence rate is actually a full order better than is guaranteed by theory for such lowest order elements on fourth order problems.

TABLE 1

The errors $e_h = I_h u - u_h$ and orders of convergence. “#CG” refers to the number of conjugate-gradient iterations required.

	$ e_h _{L^2}$	h^r	$ e_h _{H^1}$	h^r	$ e_h _{H^2}$	h^r	#CG
2	0.04236452481	0.0	0.44694944	0.0	3.51681	0.0	5
3	0.00628333081	2.8	0.13347184	1.7	1.99699	0.8	30
4	0.00080789569	3.0	0.03454516	1.9	1.03066	1.0	86
5	0.00010160485	3.0	0.00870494	2.0	0.51920	1.0	291
6	0.00001271921	3.0	0.00218044	2.0	0.26008	1.0	1071
7	0.00000159048	3.0	0.00054537	2.0	0.13010	1.0	4219

REFERENCES

- [1] J. ALBERTY, *Nonlinear Black Scholes Modelling—FDM vs. FEM*, Master’s Thesis, University of Oxford, Oxford, UK, 2004.
- [2] J. H. ARGYRIS, I. FRIED, AND D. W. SCHARPF, *The TUBA family of plate elements for the matrix displacement method*, Aeronaut. J. Roy. Aeronaut. Soc., 72 (1968), pp. 514–517.
- [3] P. G. CIARLET, *The Finite Element Method for Elliptic Problems*, North-Holland, Amsterdam, 1978.
- [4] V. GIRAULT AND L. R. SCOTT, *Hermite interpolation of nonsmooth functions preserving boundary conditions*, Math. Comp., 71 (2002), pp. 1043–1074.
- [5] Y. HUANG AND S. ZHANG, *A lowest order divergence-free finite element on rectangular grids*, Frontiers Math. China, to appear.
- [6] M. J. D. POWELL AND M. A. SABIN, *Piecewise quadratic approximations on triangles*, ACM Trans. Math. Software, 3–4 (1977), pp. 316–325.
- [7] L. L. SCHUMAKER, *Spline Functions: Basic Theory*, 3rd ed., Cambridge University Press, Cambridge, UK, 2007.
- [8] L. R. SCOTT AND S. ZHANG, *Finite element interpolation of nonsmooth functions satisfying boundary conditions*, Math. Comp., 54 (1990), pp. 483–493.
- [9] S. ZHANG, *A family of $Q_{k+1,k} \times Q_{k,k+1}$ divergence-free finite elements on rectangular grids*, SIAM J. Numer. Anal., 47 (2009), pp. 2090–2107.